Received: 9 January 2023 | Revised: 4 September 2023 | Accepted: 5 September 2023

DOI: 10.1002/asl.1190

RESEARCH ARTICLE

Atmospheric Science Letters RMetS

The link between North Atlantic tropical cyclones and ENSO in seasonal forecasts

Robert Doane-Solomon[1] | **Daniel J. Befort**[1,2] | **Joanne Camp**[3] | **Kevin Hodges**[4,5] | **Antje Weisheimer**[6,7]

[1]Atmospheric, Oceanic and Planetary Physics, Department of Physics, University of Oxford, Oxford, UK

[2]European Centre for Medium-Range Weather Forecasts (ECMWF), Bonn, Germany

[3]Met Office Hadley Centre, Exeter, UK

[4]Department of Meteorology, University of Reading, Reading, UK

[5]National Centre for Atmospheric Science, University of Reading, Reading, UK

[6]National Centre for Atmospheric Science, Atmospheric, Oceanic and Planetary Physics, Department of Physics, University of Oxford, Oxford, UK

[7]European Centre for Medium-Range Weather Forecasts (ECMWF), Reading, UK

Correspondence
Robert Doane-Solomon, Pembroke College, University of Oxford, Oxford, OX1 1DW, UK.
Email: robert.doane-solomon@pmb.ox.ac.uk

Funding information
European Commission's Horizon 2020 programme, Grant/Award Number: 776613; Met Office Academic Partnership (MOAP); NERC National Centre for Atmospheric Science

Abstract

This study assesses the ability of six European seasonal forecast models to simulate the observed teleconnection between ENSO and tropical cyclones (TCs) over the North Atlantic. While the models generally capture the basin-wide observed link, its magnitude is overestimated in all forecast models compared to reanalysis. Furthermore, the ENSO-TC relationship in the Caribbean is poorly simulated. It is shown that incorrect forecasting of wind shear appears to affect the representation of the teleconnection in some models, however it is not a completely sufficient explanation for the overestimation of the link.

KEYWORDS

ENSO, North Atlantic, seasonal forecasts, tropical cyclones

1 | INTRODUCTION

Tropical cyclones (TCs) cause significant annual losses and casualties, with North Atlantic TCs being the most destructive natural disasters in the United States (Grinsted et al., 2019). Several variables affect the interannual variability of TC numbers and their location, such as the El Niño–Southern Oscillation (ENSO; Jaramillo et al., 2021; Lin et al., 2020; Xie et al., 2005) and tropical Atlantic sea surface temperatures (Klotzbach et al., 2019). Years exhibiting La Niña conditions since 2010 have been associated with record-breaking TC activity in the North Atlantic, such as in 2020 and an extremely active season in 2017 (Klotzbach et al., 2022; Lim et al., 2018). Indeed, ENSO is thought to be the single most important factor in seasonal TC variability (Camargo et al., 2010; Chu, 2004; Gray, 1984; Yang et al., 2018). Global shifts in atmospheric and oceanic weather patterns occur in response to ENSO, due to the

Abbreviations: ENSO, El Niño–Southern Oscillation; GOM, Gulf of Mexico; JASO, July–August–September–October; MDR (-A, -C), main development region (-Atlantic, -Caribbean); TC, tropical cyclone.

strengthening/weakening of the Walker and Hadley circulations. Over the North Atlantic, ENSO impacts include changes in sea surface temperatures (Goldenberg et al., 2001), tropospheric vorticity (Camargo et al., 2007), vertical wind shear (WS) and humidity (Klotzbach, 2011). WS and humidity are thought to be the most important factors influenced by ENSO in terms of their impact on TCs, while tropospheric vorticity is thought to be less relevant in the North Atlantic compared to other basins (Camargo et al., 2007; Klotzbach, 2011). In an El Niño year WS usually increases over the Main Development Region of the tropical Atlantic (MDR—the area between 10 and 20 N and 20 and 85 W), and vice versa during La Niña years (Camargo et al., 2010). TCs can be thought of as heat engines transferring heat from warm tropical ocean waters to the cold upper atmosphere—WS suppresses a TC by dissipating the warm core structure at the top of the storm and inducing asymmetries in its circulation, making the heat engine less efficient (Frank & Ritchie, 2001; Willoughby, 1999). Consequently, TC activity usually decreases in the North Atlantic during El Niño, whereas a La Niña event usually enhances TC activity (Brown, 2006; Klotzbach, 2011). To obtain skillful seasonal forecasts of TC activity it is important to correctly represent the observed relationship between tropical Pacific sea surface temperatures and those factors impacting North Atlantic TCs, for example, WS and local SSTs.

Many operational forecasting centers produce seasonal forecasts with 6-month lead times from which predictions of TC activity can be determined. Previous studies have shown that the interannual variability of NA TCs can be predicted to some extent using such seasonal forecasts. Vitart et al. (2007) studied three seasonal forecast models from the European Seasonal to Interannual Prediction system, finding a high degree of correlation between predicted and actual NA TC numbers per season. More recently, Befort et al. (2022) analyzed the ability of six state-of-the-art operational European seasonal forecast models in simulating interannual TC variability over the NA and Western North Pacific basins during 1993 to 2014. They found that these models are skillful in simulating TC variability over the NA basin, but are generally poor over the Western North Pacific, despite significant climatological differences between the models. However, Befort et al. (2022) did not investigate the ability of the models to simulate the observed TC-ENSO teleconnection in either of these basins. ENSO forecast accuracy is a crucial factor in correctly predicting seasonal TC variations (Camargo[1] et al., 2007). Analysis of the UK Met Office Glosea5-GA3 model over the 1992–2013 period has shown a statistically significant reduction in NA TC numbers during periods of El Niño activity (Camp et al., 2015). Additionally, Vitart and Stockdale (2001) analyzed the teleconnection between ENSO and NA TCs in an early version of ECMWF's seasonal forecast system. This correctly showed fewer storms in El Niño and more in La Niña, albeit with a small sample size from 1991 to 1999.

Here, we expand on the Befort et al. (2022) study by analyzing the predictability of the TC-ENSO teleconnection in the North Atlantic for the same seasonal forecast models. This paper is structured as follows: first we assess the relationship between central equatorial Pacific SSTs and TC numbers during the active July to October (JASO) season in the different seasonal forecast models, and compare them to reanalysis and best track observations. Next, we analyze to what extent the errors in the simulated ENSO-TC relationship can be explained by local environmental variables over the tropical NA. This involves investigating the simulated link between ENSO and the interannual variability of vertical WS and humidity, and how differences between the simulated relationships may contribute to errors in the overall simulated interannual variability of TCs. We specifically focus on WS and humidity due to their strong relationship with both ENSO and TC formation. We conclude by summarizing the results and discussing the limitations of the methods and data used.

2 | METHODS AND DATA

In this study, hindcast data from six different dynamical seasonal forecast models are used. These are the following six European models, which contribute to the Copernicus Climate Change Service (C3S) multimodel seasonal forecasting system: UK Met Office GloSea5-GC2 (UKMO) (MacLachlan et al., 2015), German Weather Service GCFS2.0 (DWD; Fröhlich et al., 2020), Euro-Mediterranean Center on Climate Change SPS3 (CMCC) (Gualdi et al., 2020), European Center for Medium-Range Weather Forecasts SEAS5 (ECMWF) (Johnson et al., 2019), Météo-France System 5 (MF5) and Météo-France System 6 (MF6) (Dorel et al., 2017). Details of the resolution and ensemble size of each of these models are available in Table S1. Forecasts initialized at the beginning of June during the hindcast period 1993 and 2014 are used, which results in a total of 22 TC seasons. The European Center for Medium-Range Weather Forecasts (ECMWF) fifth generation reanalysis (ERA5) (Hersbach et al., 2020) is used as a reference for the ENSO index and TC numbers, as well as for specific humidity and WS data. This reanalysis has resolution ~31 km, similar to that of the highest resolution forecast models in this study (Table S1). The same tracking and detection methods are used to identify TCs in ERA5 and the seasonal forecast models. Observational TC data from the International Best

Track Archive for Climate Stewardship (IBTrACS; Knapp et al., 2010, 2018) is also used as an additional reference for TC counts. IBTrACS is a dataset of historical storms' location and intensity, interpolated to 3-h intervals with 0.1° resolution. We sub-sample these data to 12-h intervals to be consistent with the seasonal forecasting systems.

The TCs in ERA5 and the seasonal forecast models are tracked using the methods described in Hodges et al. (2017). Potential TCs are first identified using the vertical average of vorticity between 850 and 700 hPa, spectrally filtered to T63 with the large scale background removed, and a threshold of $5 \times 10^{-6}\,s^{-1}$. As the same T63 spectral filter is applied to all seasonal forecasts, the influence of model resolution in the identification of the TCs is reduced. The potential cyclones are then used to track the motion of the storms. By minimizing a cost function subject to adaptive constraints, smooth storm trajectories are produced (Hodges, 1994, 1995, 1999). TCs are then identified by using the same criteria as in Befort et al. (2022) and Hodges et al. (2017):

1. The T63 relative vorticity at 850 hPa must be at least $6 \times 10^{-5}s^{-1}$.
2. The T63 vorticity difference between 850 and 200 hPa must be at least $6 \times 10^{-5}s^{-1}$.
3. There must be a T63 vorticity center at each level between 850 and 200 hPa for which there are data.
4. The above criteria must apply for a minimum of two consecutive timesteps (1 day), over the ocean.
5. Tracks must start between 0 N and 30 N.

The TC tracks generated correspond to the entire lifecycle of all storms that develop into TCs: this includes if/when they are African easterly waves. We do not apply any additional intensity thresholds for genesis to the TCs in order to retain consistency across the models, as this would be very resolution dependent (Camargo, 2013; Horn et al., 2014). Gridded track density statistics are calculated using the spherical kernel estimators described in Hodges (1996). The unit for track density in the figures is storms per ensemble member per unit area per season, where the unit area is a 5° spherical cap ($\approx 10^6$ km^2). The JASO (July–August–September–October) period is used for all analysis, being the most active season over the NA basin (Befort et al., 2022; Saunders et al., 2000). The Niño 3.4 region (5 S–5 N and 170 W–120 W) is used for the ENSO index in our analysis. The index used here is equivalent to the SST anomaly in this region, using 1993–2014 as the baseline (Niño 3.4 index). Study of the North Atlantic is performed basin-wide, with particular interest paid to the following three regions: main development region—Atlantic (MDR-A; 10–20 N and 20–60 W), main development region—Caribbean (MDR-C; 10–20 N and 60–85 W) and Gulf of Mexico (GOM; 20–30 N and 100–80 W; Burn & Palmer, 2015; Ercolani et al., 2015). These regions have high TC track densities and/or landfall potential (Weinkle et al., 2012). In maps of the basin, areas are masked where the annual average TC track density for that model is <1 storm per ensemble member per season per unit area. This helps the analysis by removing areas with low TC count. We also mask out the Eastern Pacific basin.

This study focuses on the TC-ENSO teleconnection. The relationships such as TC-WS, WS-ENSO, TC-humidity, and humidity-ENSO are also analyzed. Here, the average monthly vertical WS is calculated using the following formula:

$$\mathrm{WS} = \sqrt{(\overline{u_{200}} - \overline{u_{850}})^2 + (\overline{v_{200}} - \overline{v_{850}})^2}$$

where $\overline{u}$ and $\overline{v}$ refer to the monthly averaged zonal and meridional winds, and the subscript refers to the pressure level. The forecast model performance is assessed by comparing the linear correlation and regression coefficients from the forecasts with those from ERA5 and IBTrACS. When correlations and regressions are calculated between IBTrACS TC numbers and another variable (e.g., ENSO Index), we use ERA5 data for the other variable. Spatial statistics are generated by calculating temporal correlation coefficients between two variables at each grid point (e.g., WS and TC numbers), or between one variable and the ENSO Index. Bootstrapping is used to provide an estimate of the uncertainty of regressions and correlations. This is done by resampling the target data 1000 times with replacement. For the purposes of this study, the values at the 10th and 90th percentiles of a bootstrapped distribution were used to provide estimates of upper and lower bounds for that value.

TC track composites of El Niño years and La Niña years (as predicted by that model) were also used to investigate any nonlinear behavior. Due to the different variance of the ENSO Index across the models, we scale the model ENSO indices to have the same variance as the ERA5 ENSO Index. For a given model, El Niño years are defined as a scaled JASO ENSO index >0.5°C, or <−0.5°C for La Niña years. These years are shown in Table S2.

3 | RESULTS

3.1 | Impact of ENSO on TC numbers

We initially investigate the relationship between ENSO and North Atlantic TCs on a basin-wide scale (Figure 1).

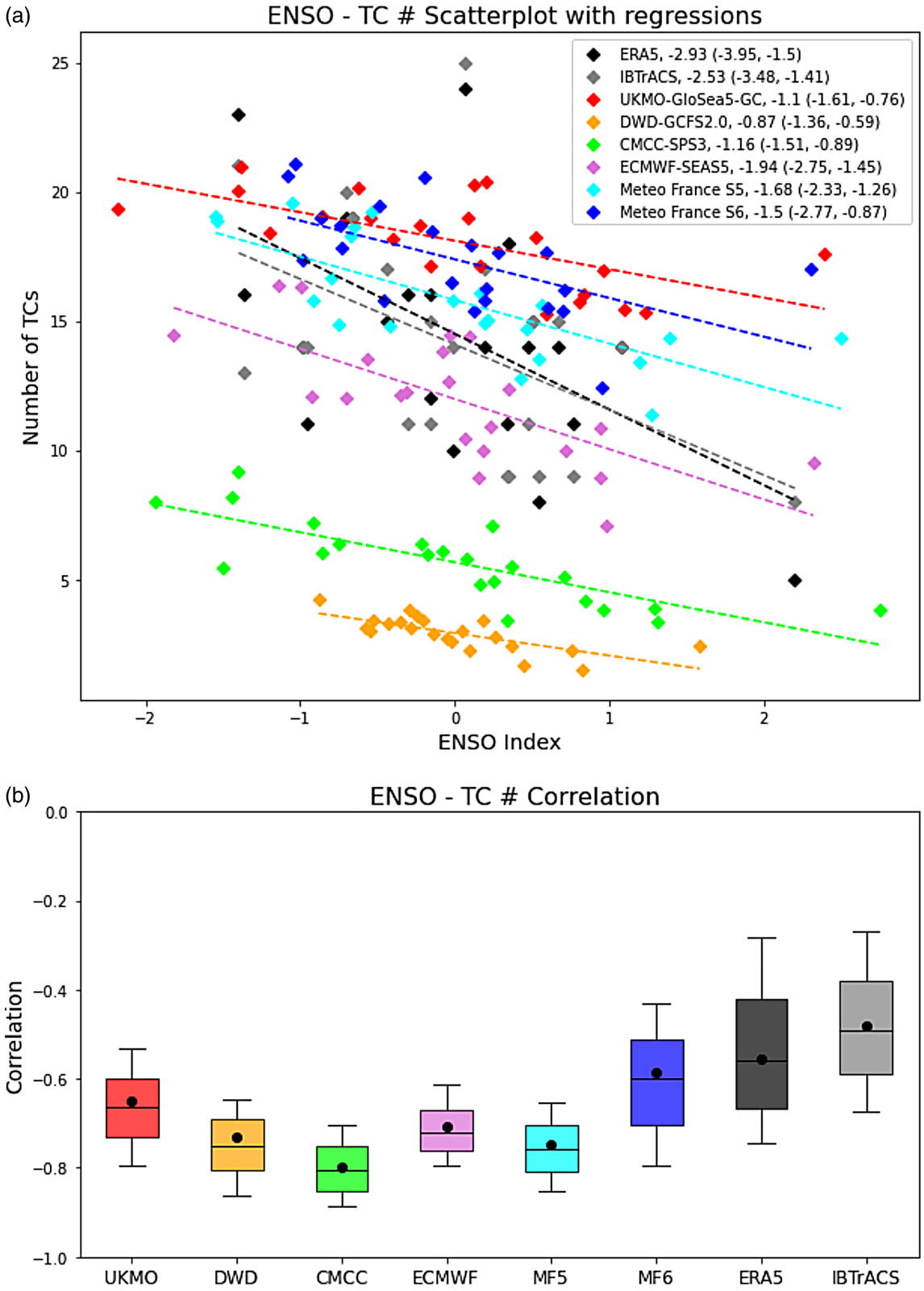

FIGURE 1 (a) Scatterplot of number of TCs in the North Atlantic basin for JASO from 1993 to 2014 versus NINO 3.4 SST Index for IBTrACS (gray), reanalysis (black), and the seasonal forecast models (colors). Values in the legend are the regression coefficient between the two variables, and the values in brackets are the 10th and 90th percentiles of the bootstrapped regression distribution. (b) Correlation between the number of TCs in the North Atlantic basin for JASO from 1993 to 2014 and NINO 3.4 SST index. The box and whisker plot shows the bootstrapped distribution of the correlation, with the whiskers at the 10th and 90th percentiles.

As shown in Figure 1a, a negative relationship between the ENSO Index and TC numbers is found when using IBTrACS or tracks identified in ERA5, which is in agreement with previous studies (Brown, 2006; Klotzbach, 2011). All six forecast models capture the negative relationship between ENSO and TC numbers, despite the fact that some models (DWD and CMCC) have significant negative biases in TC numbers (also see Figure S1). The magnitude of the regression coefficient (shown in the legend of Figure 1a) between ENSO and TC numbers ranges from ~ -2.5 to -3 in IBTrACS and ERA5 and ~ -1 to -2 in the models. Figure 1b shows the correlation coefficient, with the whiskers of the boxplots corresponding to the correlation coefficients at the 10th and 90th percentiles of the bootstrapped distribution. For all the seasonal forecast models, the absolute correlation value is larger than for ERA5 and IBTrACS, but there is a large uncertainty. In contrast, the absolute value of the regression coefficients in the forecasts are all smaller in magnitude than in ERA5 and IBTrACS. This discrepancy is likely due to the interannual variability of the ensemble mean number of storms being much lower in the models. As correlations are less influenced by the differences in interannual variability of TC numbers across the models, this motivates the use of correlations over regressions in the rest of the study. Furthermore, the similarity of the correlation and regression values (and their respective uncertainty) between ERA5 and IBTrACS in Figure 1 motivates the use of ERA5 alone as the comparison in the following plots, as well as the fact that the same tracking scheme has been used for ERA5 and the models.

We next analyze the effect of ENSO on the TC spatial pattern across the basin. First, we show average JASO track densities across the basin in Figure 2. The ERA5 data show the MDR-A (the central Atlantic between 10 and 20 N) is the most active region for TC development. Many storms there track north-westwards and recurve in the open Atlantic, while some move westwards into the MDR-C (the Caribbean). In the western part of MDR-C and the GOM, an area of enhanced activity is also seen. A similar pattern in MDR-A is seen in the models, however some models (UKMO, MF6) have too large a proportion of storms on a recurving track while others appear slightly too zonal (MF5). As in Figure 1a, we see that the DWD and CMCC models produced far fewer storms than ERA5. It also appears from the track densities that UKMO and MF6 produce fewer storms than ERA5, in contrast to the storm counts shown in Figure 1a. However, the high track density off Africa in ERA5 is likely due to more storms originating over the African coastal region and being more tightly constrained. In the models there are fewer storms in this region and they are more spread out, which leads to a lower track density. The adaptive smoothing method used (Hodges, 1996) may also contribute to this effect.

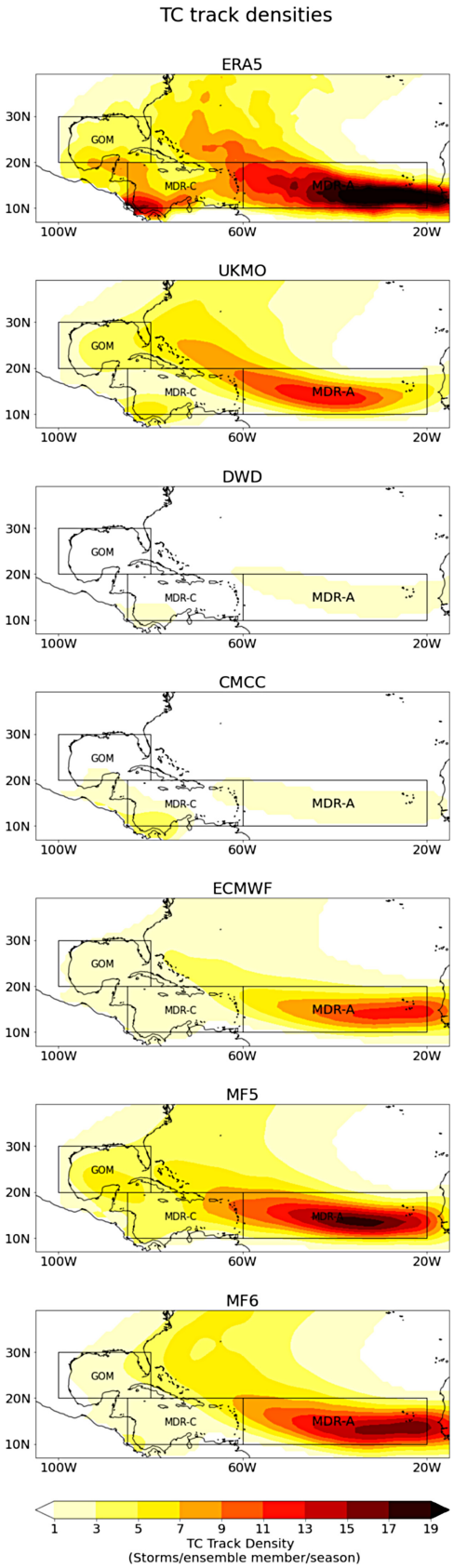

FIGURE 2 Map of JASO TC track densities from ERA5 and the six seasonal forecast models for the period JASO 1993–2014. Units are storms per unit area (5° spherical cap) per season per ensemble member.

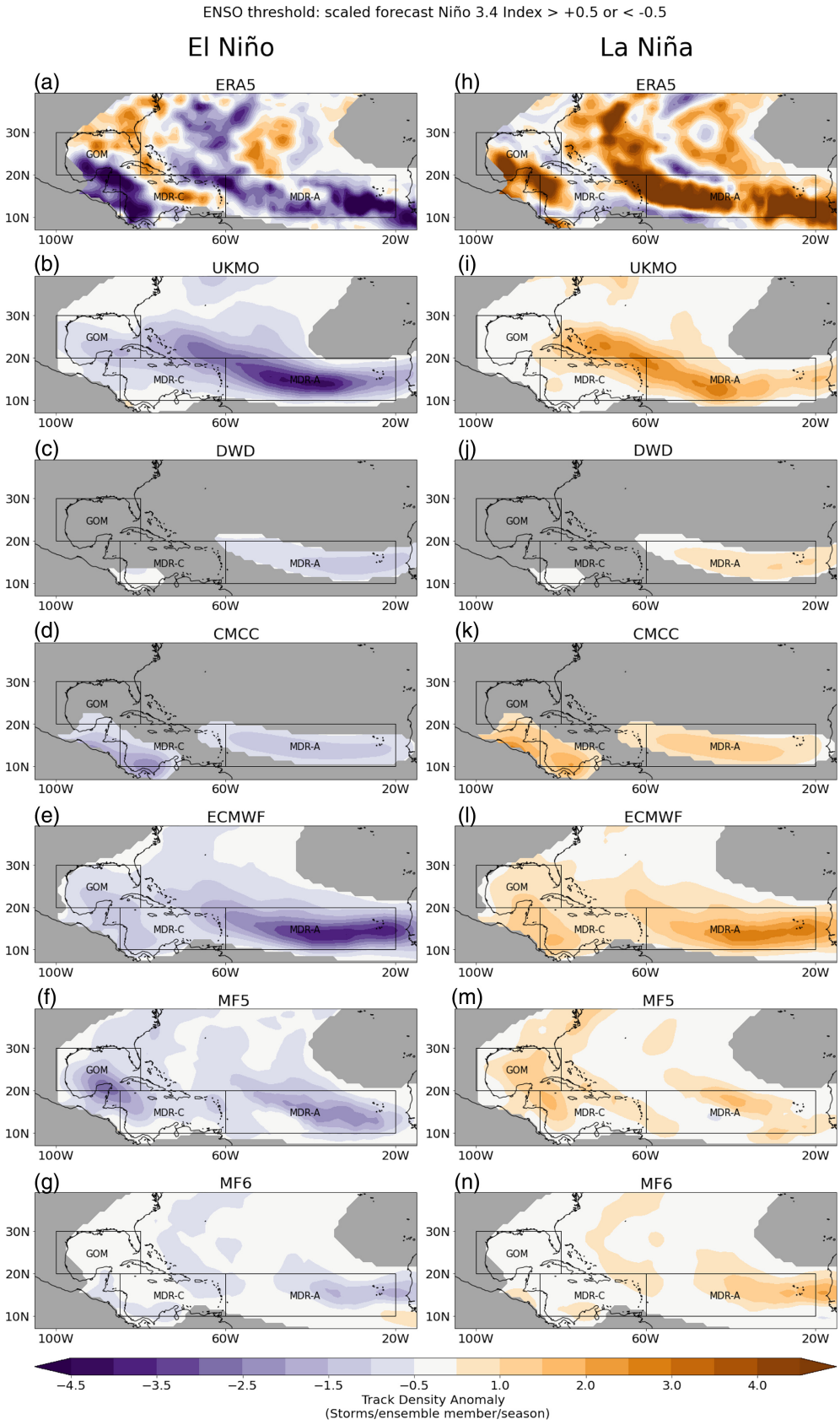

FIGURE 3 ENSO track composites for El Niño (a–g) and La Niña (h–n). Map of track density anomalies during El Niño and La Niña years predicted by the respective model. Panels (a) and (h) for ERA5 reanalysis data and all other panels for seasonal forecast models. Areas are masked where the annual average track density for that model is <1 storm/ensemble member/season/unit area. The ENSO threshold is the scaled forecast Niño 3.4 index for JASO >0.5°C or <−0.5°C.

Track density changes during El Niño and La Niña events are shown in Figure 3. In ERA5, El Niño years exhibit lower track density in two main areas: one over the MDR-A and recurving northwards, and another in the western MDR-C and GOM. They are separated by an area of increased TC activity in the eastern MDR-C and

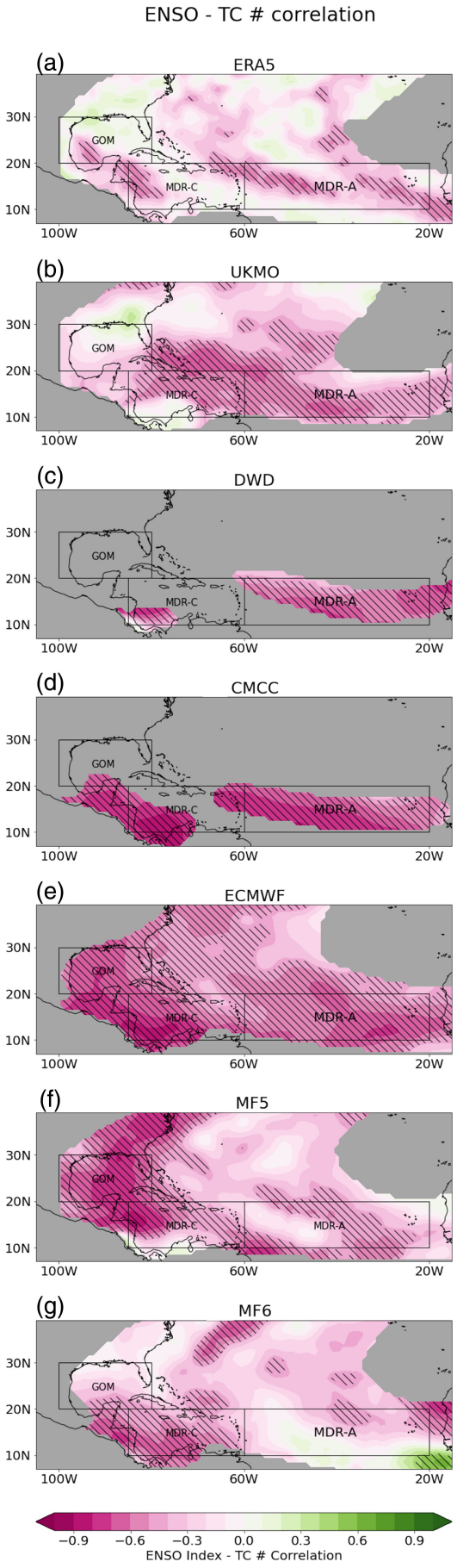

near Florida. This pattern is potentially associated with El Niño Modoki, where the focus of warming is shifted to the central Pacific (Wang et al., 2014). However, Modoki events have become more frequent in recent years (Wang et al., 2017), so the strength of the signal seen in ERA5 may be related to the period used (1993–2014). We find a smaller but still noticeable anomaly when analyzing the longer period from 1979 to 2017 (Figure S2). All models capture the basin-wide reduction in TC activity during El Niño years, but are unable to capture the finer spatial pattern described above. During El Niño years, no model with sufficient storm counts shows an increase anywhere over the MDR-C. For La Niña years in ERA5 (Figure 3h), we find TC track density anomalies are nearly the opposite of the response obtained during El Niño years. During La Niña, we see an increase in storm count over the MDR-A and in the western MDR-C and GOM, and a small decrease in the eastern MDR-C and near Florida. The models do not capture this pattern, but the basin-wide average response is captured well during La Niña years. Despite the low annual track density in DWD and CMCC, a notable track density anomaly is still observed over the MDR-A in both models, indicating a large ENSO impact.

In Figure 1 we saw that the interannual variability between basin-wide TC counts and ENSO is well represented in the models. To further investigate this relationship, we examine the spatial structure of this correlation across the basin (Figure 4). ERA5 displays a statistically significant negative correlation in MDR-A and the western MDR-C and GOM regions. This is in line with the basin-wide results in Figure 1. Most forecast models in general simulate well the strong negative correlation in MDR-A (except for MF6). However, some models show a stronger negative correlation near Florida and in MDR-C, which is not found in ERA5. We also note that some models predict an area of significant negative correlation around 30 N, although the size and location of this differs between them. Such a signal is not seen in ERA5. Along with the results from Figure 3, this provides further evidence that despite the correct sign of the ENSO response being seen on average across the basin, all

FIGURE 4 ENSO-TC correlation map. Correlation coefficient of interannual variability between NINO 3.4 SST index and number of TCs in the North Atlantic basin for JASO from 1993 to 2014. Panel (a) for ERA5 reanalysis data and panels (b–g) for the seasonal forecast models. Areas are masked where the annual average track density for that model is <1 storm/ensemble member/season/unit area. Shaded areas correspond to correlations significant at the 5% level.

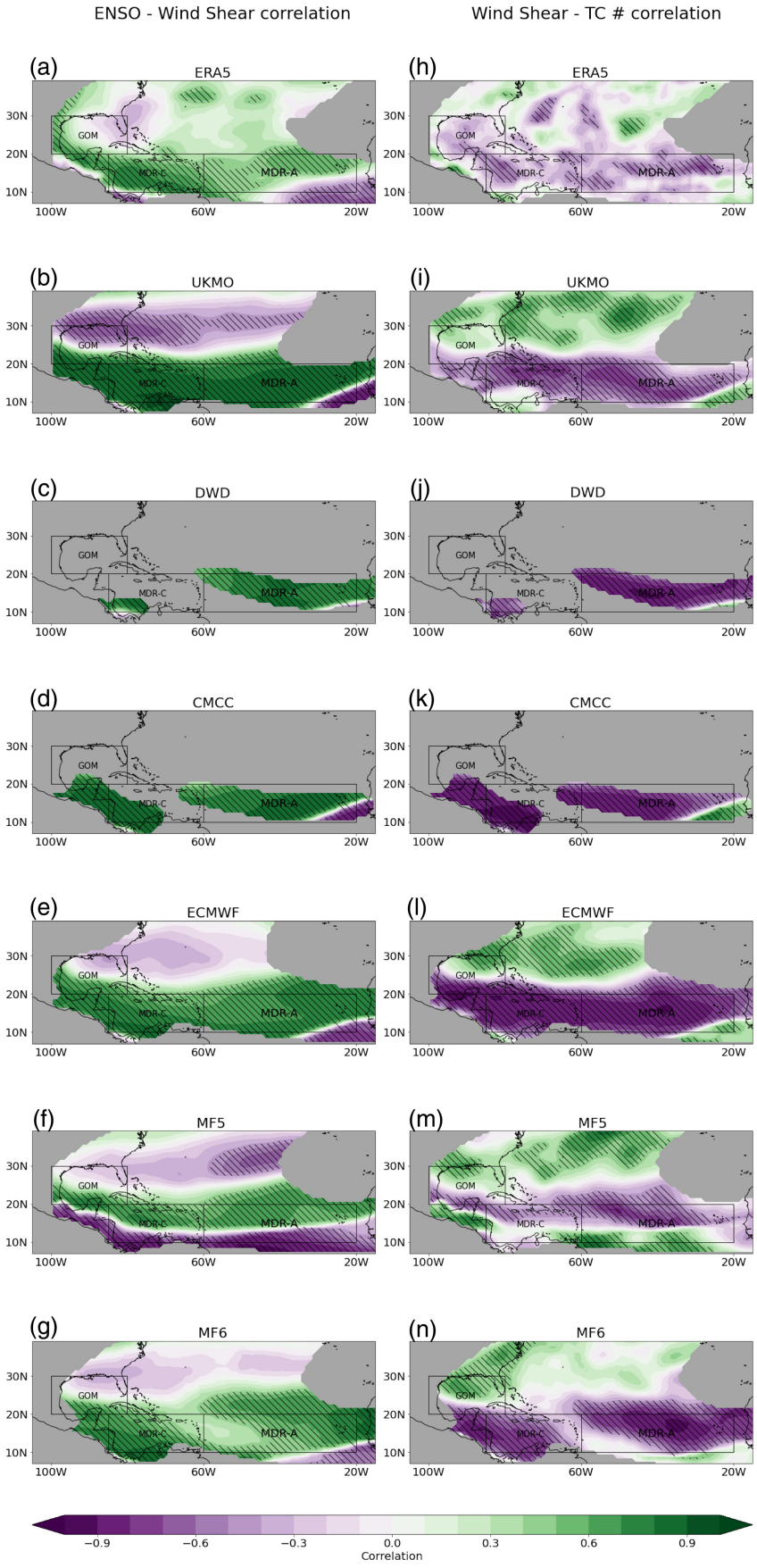

FIGURE 5 ENSO-WS and WS-TC correlations. Left column: Correlation coefficients of interannual variability between NINO 3.4 SST index and WS in the North Atlantic basin for JASO from 1993 to 2014. Right column: Correlation coefficients of interannual variability between WS and total number of TCs in the North Atlantic basin for the same period. Panels (a) and (h) for ERA5 reanalysis data and all other panels for the seasonal forecast models. Areas are masked where the annual average track density for that model is <1 storm/ensemble member/season/unit area. Shaded areas correspond to correlations significant at the 5% level.

analyzed forecast models have difficulties representing the details of the spatial pattern of the ENSO-TC teleconnection over the North Atlantic.

3.2 | Relationship between ENSO, TC numbers, and environmental variables

To explore what might be causing some of the errors found in the TC-ENSO relationship in the different models, we examine the effect of environmental variables that link the ENSO SST with the atmospheric conditions required for the formation of TCs in the NA basin. WS and humidity are the variables most heavily influenced by ENSO. For example, during El Niño the Walker circulation shifts eastwards, leading to stronger high-altitude westerly winds within the Hadley cell, and descending dry air over the Caribbean. This suppresses the formation of TCs (Camargo et al., 2010; Klotzbach, 2011).

The correlations between ENSO and WS, and between WS and TC numbers, are shown in Figure 5. The ERA5 reanalysis (Figure 5a) shows a positive correlation between ENSO Index and WS across most of the Atlantic basin, except for the wider region around Florida. WS is generally negatively correlated with TC numbers across the basin, as expected (Gray, 1968). This is replicated in the models south of 25 N, with slight shifts in location and intensity. The magnitude of the WS-TC correlation is overestimated over the MDR-A for all models, except for MF5 and MF6, which show a large region with little correlation. However, the observed ENSO-WS/WS-TC relationship north of 25 N is uniformly poorly simulated by the models with a notable storm count in this region. They display a sharp transition in the sign of the correlation coefficient, in contrast to ERA5.

As moist air is another crucial element for TC development and is known to be affected by ENSO, we performed the same analysis for 500 hPa specific humidity. The results are available in the Figure S5; however, it was judged that errors in forecast models' representation of the ENSO-TC teleconnection was more likely due to WS than humidity. This is because in the locations with the largest errors in the ENSO-TC correlation, the ENSO-humidity, and humidity-TC correlations are generally well simulated (around 30 N and over the MDR-C).

4 | CONCLUSION AND DISCUSSION

We expand on a recent study by Befort et al. (2022), analyzing the performance of six European seasonal forecast models at predicting the TC-ENSO teleconnection in the North Atlantic. Basin-wide, it is found that the observed negative correlation between the Niño 3.4 ENSO Index and the total number of TC counts over the (JASO) season is well predicted by the models. Over the MDR-A, the sign of the TC-ENSO correlation coefficient in Figure 4 is forecasted correctly for all models except MF6. In the eastern Caribbean and near Florida, the models simulate a strong linear relationship between TC numbers and ENSO Index that is not present in ERA5. This may be due to the short data record, however similar errors are found by Wang et al. (2014) when analyzing the response of global climate models to El Niño Modoki events. They find that multiple models do not simulate an increase in TC counts near Florida during El Niño Modoki (their Figures 2e and 6), which they partially attribute to errors in simulating WS. In our analysis, we see no firm evidence that WS and humidity drive the differences in the track density anomaly in MDR-C between the models and ERA5 (Figure 3). The magnitude of the TC-ENSO correlation in Figure 4 is generally too strong in the forecasts, especially between 10 and 20 N. However, the number of ensemble members in the forecast models likely leads to higher correlations in forecast models compared to ERA5.

Over the MDR, we find that the observed ENSO-WS and WS-TC correlations are generally well simulated by the forecast models (Figure 5). However, the correlation coefficients in the models north of 25 N are the opposite sign to those in ERA5. The sharpness of the transition in the sign of the ENSO-WS correlation coefficient around 25 N may be due to errors simulating the Hadley cell's response to ENSO. It is believed that the northern edge of the Hadley cell usually moves south during El Niño and north during La Niña (Hu et al., 2018; Lu et al., 2008; Wang, 2004). In theory, this would lead to a strong correlation between ENSO and WS in the tropics inside the Hadley cell, with a smooth decrease to an area of no correlation on the north side of the boundary. As this is not seen in the models, the sharp decrease may be due them failing to alter the width of the Hadley cell in response to ENSO, keeping the edge location fixed. The incorrect modeling of the edge of the Hadley cell may cause the pattern seen in the simulated correlation between WS and TCs, which is strongly positive in the subtropics despite the physical effect of WS causing storms to weaken and dissipate. This is not seen in ERA5, which has a weak negative correlation almost throughout the NA basin. Together, this may explain the areas of negative correlation seen in the subtropics in the overall ENSO-TC correlation (Figure 4).

In general, it is found that the forecast models with higher levels of annual TC activity (i.e., UKMO, ECMWF, MF5, and MF6) simulate significant correlations between the environmental variables and TC numbers for larger areas of the North Atlantic than can be detected in

reanalysis data. This is possibly due to the fact that there is only one realization for each year in ERA5 compared to tens of ensemble members for each year in the models, which are combined into the ensemble mean (see Figure S4 for an analysis using individual ensemble members). Thus, it is likely that the area of significant correlations with TC numbers is larger in these forecast models because the number of TC tracks is much larger.

Overall, this analysis shows that the basin-wide TC-ENSO teleconnection is well represented by these six seasonal forecast models between 1993 and 2014. Due to the observed relationship between ENSO and TCs in the NA basin, an important question is whether models that more accurately simulate the ENSO-TC teleconnection are more accurate at predicting basin-wide or sub-regional TC frequency. We investigated this in Figure S6 but no strong relationship was found. There is considerable uncertainty due to the large interannual variability and short hindcast period of only 22 years. Thus, the question of whether a good representation of the observed ENSO-TC relationship in the models is an important factor for TC skill cannot be answered with the set of simulations used in this study. This emphasizes the importance of generating longer hindcasts for the seasonal forecast systems. For some systems, such as ECMWF, more extensive hindcasts do exist. We intend to use the longer ECMWF CSF-20C hindcasts (Weisheimer et al., 2020), which cover the period 1901–2010, to study these questions of skill in the future.

AUTHOR CONTRIBUTIONS

Robert Doane-Solomon: Data curation; formal analysis; investigation; methodology; visualization; writing – original draft. **Daniel J. Befort:** Conceptualization; data curation; project administration; resources; supervision; writing – review and editing. **Joanne Camp:** Project administration; supervision; writing – review and editing. **Kevin Hodges:** Data curation; formal analysis; methodology; writing – review and editing. **Antje Weisheimer:** Conceptualization; investigation; methodology; supervision; writing – review and editing.

ACKNOWLEDGEMENTS

We thank the reviewers for their useful suggestions on how to improve this manuscript. We are grateful for the support received from the Met Office Academic Partnership (MOAP). Robert Doane-Solomon received funding from MOAP. Daniel J. Befort and Antje Weisheimer received funding from the European Union under Horizon 2020 (Grant Agreement 776613. Kevin Hodges was funded as part of the NERC National Centre for Atmospheric Science. All reanalysis and seasonal forecast data are available from the C3S website (https://climate.copernicus.eu). Tropical cyclone track data are available upon request for the seasonal forecast models and reanalysis. IBTrACS data are available at https://www.ncei.noaa.gov/products/international-best-track-archive.

FUNDING INFORMATION

RDS was funded by the Met Office Academic Partnership (MOAP). DJB and AW were supported by the EUCP project funded by the European Commission's Horizon 2020 programme, Grant Agreement number 776613. KH was funded as part of the NERC National Centre for Atmospheric Science.

CONFLICT OF INTEREST STATEMENT

All authors declare no conflicts of interest.

ORCID

Robert Doane-Solomon https://orcid.org/0000-0002-7428-4398
Daniel J. Befort https://orcid.org/0000-0002-2851-0470
Joanne Camp https://orcid.org/0000-0002-4567-9622
Kevin Hodges https://orcid.org/0000-0002-7724-5271
Antje Weisheimer https://orcid.org/0000-0002-7231-6974

REFERENCES

Befort, D.J., Hodges, K.I. & Weisheimer, A. (2022) Seasonal prediction of tropical cyclones over the North Atlantic and Western North Pacific. *Journal of Climate*, 35, 1385–1397.

Brown, M.E. (2006) Hurricanes and typhoons: past, present, and future. *Southeastern Geographer*, 46, 323–324.

Burn, M.J. & Palmer, S.E. (2015) Atlantic hurricane activity during the last millennium. *Scientific Reports*, 5, 1–11.

Camargo, S.J. (2013) Global and regional aspects of tropical cyclone activity in the CMIP5 models. *Journal of Climate*, 26, 9880–9902.

Camargo, S.J., Emanuel, K.A. & Sobel, A.H. (2007) Use of a genesis potential index to diagnose ENSO effects on tropical cyclone genesis. *Journal of Climate*, 20, 4819–4834.

Camargo, S.J., Sobel, A.H., Barnston, A.G. & Klotzbach, P.J. (2010) *The influence of natural climate variability on tropical cyclones, and seasonal forecasts of tropical cyclone activity*. Singapore: World Scientific, pp. 325–360. Available from: https://doi.org/10.1142/9789814293488_0011

Camargo1, S.J., Barnston, A.G., Klotzbach, P.J. & Landsea, C.W. (2007) Seasonal tropical cyclone forecasts. *WMO Bulletin*, 56, 297.

Camp, J., Roberts, M., MacLachlan, C., Wallace, E., Hermanson, L., Brookshaw, A. et al. (2015) Seasonal forecasting of tropical storms using the met Office GloSea5 seasonal forecast system. *Quarterly Journal of the Royal Meteorological Society*, 141, 2206–2219.

Chu, P.-S. (2004) *ENSO and tropical cyclone activity*. New York: Columbia University Press.

Dorel, L., Ardilouze, C., Batté, L., Déqué, M. & Guérémy, J. (2017) *Documentation of the 631 Météo-France pre-operational seasonal forecasting system*. Météo-France Technical Report 401. Reading, UK: ECMWF.

Ercolani, C., Muller, J., Collins, J., Savarese, M. & Squiccimara, L. (2015) Intense Southwest Florida hurricane landfalls over the past 1000 years. *Quaternary Science Reviews*, 126, 17–25.

Frank, W.M. & Ritchie, E.A. (2001) Effects of vertical wind shear on the intensity and structure of numerically simulated hurricanes. *Monthly Weather Review*, 129, 2249–2269.

Fröhlich, K., Dobrynin, M., Isensee, K., Gessner, C., Paxian, A., Pohlmann, H. et al. (2020) The German climate forecast system: GCFS. *Earth and Space Science Open Archive*, 28, 1–28. Available from: https://doi.org/10.1002/essoar.10502582.1

Goldenberg, S.B., Landsea, C.W., Mestas-Nunez, A.M. & Gray, W.M. (2001) The recent increase in Atlantic hurricane activity: causes and implications. *Science*, 293, 474–479.

Gray, W.M. (1968) Global view of the origin of tropical disturbances and storms. *Monthly Weather Review*, 96, 669–700.

Gray, W.M. (1984) Atlantic seasonal hurricane frequency. Part II: forecasting its variability. *Monthly Weather Review*, 112, 1669–1683.

Grinsted, A., Ditlevsen, P. & Christensen, J.H. (2019) Normalized US hurricane damage estimates using area of total destruction, 1900-2018. *Proceedings of the National Academy of Sciences*, 116, 23942–23946.

Gualdi, S., Borrelli, A., Cantelli, A., Davoli, G., Mar Chavesmontero, M.D., Masina, S. et al. (2020) *The new CMCC operational seasonal prediction system*. Lecce, Italy: CMCC Research Paper.

Hersbach, H., Bell, B., Berrisford, P., Hirahara, S., Horanyi, A., Munoz-Sabater, J. et al. (2020) The ERA5 global reanalysis. *Quarterly Journal of the Royal Meteorological Society*, 146, 1999–2049.

Hodges, K. (1995) Feature tracking on the unit sphere. *Monthly Weather Review*, 123, 3458–3465.

Hodges, K. (1996) Spherical nonparametric estimators applied to the UGAMP model integration for AMIP. *Monthly Weather Review*, 124, 2914–2932.

Hodges, K. (1999) Adaptive constraints for feature tracking. *Monthly Weather Review*, 127, 1362–1373.

Hodges, K., Cobb, A. & Vidale, P.L. (2017) How well are tropical cyclones represented in reanalysis datasets? *Journal of Climate*, 30, 5243–5264.

Hodges, K.I. (1994) A general method for tracking analysis and its application to meteorological data. *Monthly Weather Review*, 122, 2573–2586.

Horn, M., Walsh, K., Zhao, M., Camargo, S.J., Scoccimarro, E., Murakami, H. et al. (2014) Tracking scheme dependence of simulated tropical cyclone response to idealized climate simulations. *Journal of Climate*, 27, 9197–9213.

Hu, Y., Huang, H. & Zhou, C. (2018) Widening and weakening of the Hadley circulation under global warming. *Science Bulletin*, 63, 640–644. Available from: S2095927318301919.

Jaramillo, A., Dominguez, C., Raga, G. & Quintanar, A.I. (2021) The combined QBO and ENSO influence on tropical cyclone activity over the North Atlantic Ocean. *Atmosphere*, 12, 1588.

Johnson, S.J., Stockdale, T.N., Ferranti, L., Balmaseda, M.A., Molteni, F., Magnusson, L. et al. (2019) SEAS5: the new ECMWF seasonal forecast system. *Geoscientific Model Development*, 12, 1087–1117. Available from: 12/1087/2019/.

Klotzbach, P., Blake, E., Camp, J., Caron, L.-P., Chan, J.C., Kang, N.-Y. et al. (2019) Seasonal tropical cyclone forecasting. *Tropical Cyclone Research and Review*, 8, 134–149.

Klotzbach, P.J. (2011) El Niño-southern Oscillation's impact on Atlantic Basin hurricanes and U.S. landfalls. *Journal of Climate*, 24, 1252–1263. Available from: 24/4/2010jcli3799.1.xml.

Klotzbach, P.J., Wood, K.M., Bell, M.M., Blake, E.S., Bowen, S.G., Caron, L.-P. et al. (2022) A hyperactive end to the Atlantic hurricane season October-November 2020. *Bulletin of the American Meteorological Society*, 103, E110–E128.

Knapp, K.R., Diamond, H.J., Kossin, J.P., Kruk, M.C. & Schreck, C.J. (2018) *International best track archive for climate stewardship (IBTrACS) project, Version 4. [North Atlantic]*. Asheville, NC: National Centers for Environmental Information. Available from: https://doi.org/10.25921/82ty-9e16

Knapp, K.R., Kruk, M.C., Levinson, D.H., Diamond, H.J. & Neumann, C.J. (2010) The international best track archive for climate stewardship (IBTrACS): unifying tropical cyclone data. *Bulletin of the American Meteorological Society*, 91, 363–376. Available from: 91/3/2009bams2755_1.xml.

Lim, Y.-K., Schubert, S.D., Kovach, R., Molod, A.M. & Pawson, S. (2018) The roles of climate change and climate variability in the 2017 Atlantic hurricane season. *Scientific Reports*, 8, 1–10.

Lin, I.-I., Camargo, S.J., Patricola, C.M., Boucharel, J., Chand, S., Klotzbach, P. et al. (2020) *ENSO and tropical cyclones*, Vol. 17. American Geophysical Union (AGU). Washington, DC: John Wiley & Sons, Inc., pp. 377–408. Available from: https://doi.org/10.1002/9781119548164.ch17

Lu, J., Chen, G. & Frierson, D.M. (2008) Response of the zonal mean atmospheric circulation to El Niño versus global warming. *Journal of Climate*, 21, 5835–5851.

MacLachlan, C., Arribas, A., Peterson, K.A., Maidens, A., Fereday, D., Scaife, A. et al. (2015) Global seasonal forecast system version 5 (GloSea5): a high-resolution seasonal forecast system. *Quarterly Journal of the Royal Meteorological Society*, 141, 1072–1084.

Saunders, M., Chandler, R., Merchant, C. & Roberts, F. (2000) Atlantic hurricanes and NW Pacific typhoons: ENSO spatial impacts on occurrence and landfall. *Geophysical Research Letters*, 27, 1147–1150.

Vitart, F., Huddleston, M.R., Déqué, M., Peake, D., Palmer, T.N., Stockdale, T.N. et al. (2007) Dynamically-based seasonal forecasts of Atlantic tropical storm activity issued in June by EUROSIP. *Geophysical Research Letters*, 34, 1–5.

Vitart, F. & Stockdale, T.N. (2001) Seasonal forecasting of tropical storms using coupled GCM integrations. *Monthly Weather Review*, 129, 2521–2537.

Wang, C. (2004) *The Hadley circulation: present, past and future*. Dordrecht, The Netherlands: Kluwer Academic Publishers, pp. 173–202.

Wang, C., Deser, C., Yu, J.-Y., DiNezio, P. & Clement, A. (2017) *El Niño and southern oscillation (ENSO): A Review*. Dordrecht: Springer Netherlands, pp. 85–106. Available from: https://doi.org/10.1007/978-94-017-7499-4_4

Wang, H., Long, L., Kumar, A., Wang, W., Schemm, J.-K.E., Zhao, M. et al. (2014) How well do global climate models simulate the variability of Atlantic tropical cyclones associated with ENSO? *Journal of Climate*, 27, 5673–5692. Available from: 27/15/jcli-d-13-00625.1.xml.

Weinkle, J., Maue, R. & Pielke, R., Jr. (2012) Historical global tropical cyclone landfalls. *Journal of Climate*, 25, 4729–4735.

Weisheimer, A., Befort, D.J., MacLeod, D., Palmer, T., O'Reilly, C. & Strammen, K. (2020) Seasonal forecasts of the twentieth century. *Bulletin of the American Meteorological Society*, 101, E1413–E1426. Available from: 101/8/bamsD190019.xml.

Willoughby, H. (1999) Hurricane heat engines. *Nature*, 401, 649–650.

Xie, L., Yan, T., Pietrafesa, L.J., Morrison, J.M. & Karl, T. (2005) Climatology and interannual variability of North Atlantic hurricane tracks. *Journal of Climate*, 18, 5370–5381.

Yang, S., Li, Z., Yu, J.-Y., Hu, X., Dong, W. & He, S. (2018) El Niño-southern oscillation and its impact in the changing climate. *National Science Review*, 5, 840–857.

SUPPORTING INFORMATION

Additional supporting information can be found online in the Supporting Information section at the end of this article.

How to cite this article: Doane-Solomon, R., Befort, D. J., Camp, J., Hodges, K., & Weisheimer, A. (2024). The link between North Atlantic tropical cyclones and ENSO in seasonal forecasts. *Atmospheric Science Letters*, *25*(1), e1190. https://doi.org/10.1002/asl.1190